Research

Corner cutting accuracy for thin-walled CFRPC parts using HS-WEDM

Mohamed AbouHawa[1] 🆔 · Abeer Eissa[1]

Abstract

Carbon Fiber-Reinforced polymer (CFRP) composite parts with thin-walled corners are in great demand in aircraft, cars, and precision instruments. Nonetheless, the fabrication of these parts is difficult due to their low stiffness. High-speed WEDM is an advanced technique for cutting thin CFRP components as it is a non-contact method for removing materials. Nonetheless, testing results demonstrate an unavoidable deformation in the thin-walled corners of the CFRP composite. The objective of this study is to improve the accuracy of corners in thin-walled CFRP composite parts. The research utilized a Taguchi L_{16} orthogonal array to investigate the influence of various process parameters, including pulse-on duration (P_{on}), pulse-off duration (P_{off}), and input current (I), as well as the parameter CFRP plate thickness (T), on corner inaccuracy. The CFRP thickness varied between 0.5, 1.0, 1.5, and 2.0 mm, and the corner angles examined were 30°, 60°, 90°, and 120°. Additionally, a second-order polynomial regression model was used to determine the correlation between the process parameters and corner inaccuracy at various corner angles. Also, a multi-response optimization technique using a composite desirability coupled with a generalized reduced gradient were used to find the optimal process combination across various CFRP thicknesses. According to the research findings, the most relevant process parameters impacting corner accuracy at different angles were the pulse-on duration and input current. To achieve accurate corners with different angles, the optimal process parameters were identified: P_{on} (40μs), P_{off} (15μs), and I (4A) for CFRP thicknesses 0.5 and 1.0mm, and P_{on} (45μs), P_{off} (30μs), and I (2A) for thicknesses 1.5 and 2.0mm.

Article Highlights

- HS-WEDM offers satisfactory performance in achieving precise various corner angles of thin-walled CFRP composites.
- CFRP composite thickness plays a key role in the behavior of corner cutting performance using HS-WEDM.
- The optimization method that is used improves corner accuracy by up to 30% for different CFRP thicknesses.

1 Introduction

The application of Carbon Fiber Reinforced Polymer (CFRP) composites is widespread in a variety of conventional and advanced sectors due to the demands of modern engineering and economic limitations [1]. High modulus and strength, low weight, resistance to high temperatures in conditions that oxidize, dimensional stability over a varied

✉ Mohamed AbouHawa, mohamed_abouhawa@sh-eng.menofia.edu.eg; Abeer Eissa, abeer.essa@sh-eng.menofia.edu.eg | ¹Production Engineering and Mechanical Design Department, Faculty of Engineering, Menoufia University, Shebin El Kom, Egypt.

Ⓞ Discover

temperature, good X-ray penetrability, and sufficient electromagnetic shielding are just a few of the exceptional qualities of CFRP [2, 3]. CFRP finds widespread application in wind turbines, motorbikes, bicycles, sporting goods, electrical and home appliances, drones, healthcare, aviation, military, cars, and buildings [4–6].

Chinese manufacturers have developed a variant of wire-EDM called high-speed WEDM, which is widely used in die-making. According to reports, 85% of China domestic market uses HS-WEDM [7]. Molybdenum wire is typically employed in HS-WEDM and can be reused multiple times, distinguishing it from other WEDM that dispose of the wire after a single use (Brass wire) [7]. This feature makes HS-WEDM more cost-effective. Additionally, HS-WEDM is capable of machining thick workpieces and is easy to maintain due to its simple structure. The dimensional accuracies of the machined parts improve as the tension of the wire increases, as the wire tends to vibrate during WEDM [8]. The molybdenum wire has a higher tensile strength than other wires, therefore it can withstand more stress. Its high melting point resists heat load during machining, resulting in less wire breakage. According to a study by [9], molybdenum wire in HS-WEDM produces better surface integrity compared to brass wire when used on titanium alloy. Additionally, molybdenum wire has shown improvements in cutting speed and surface roughness compared to other wires. Cutting speed is influenced by the rate of material removal and is an essential factor of WEDM [10]. Various studies have been conducted on HS-WEDM for different materials. This research focuses on achieving high corner-cutting accuracy for thin-walled CFRP parts using HS-WEDM and previously succeeded WEDM applications incorporated into a CFRP part will be presented.

Cutting CFRP composite using WEDM is a challenging task because of the heterogeneous composition of CFRP, which includes carbon fibers within a resin matrix. CFRP exhibits high strength, stiffness, and thermal resistance, but also has low electrical conductivity and high anisotropy. These material characteristics significantly affect the machinability of CFRP with WEDM. Cutting CFRP with WEDM is particularly challenging when using standard wire. Thus, previous studies [11, 12] have investigated the feasibility of employing WEDM to machine unidirectional CFRP using brass wire coated by zinc. These tests revealed that the process factors and selected wire material were appropriate for effective machining of unidirectional CFRP composites. In another investigation, it was found that the material of the wire, specifically Topas wire, resulted in higher MRR compared to Compeed wire when cutting multi-directional CFRP composite laminates [13]. An alternative method to enhance the conductivity and cutting efficiency of CFRP with WEDM involves recommending the utilization of an assisted conductive layer. The effectiveness of these conductive layers was confirmed through a demonstration showing the successful elimination of uncut epoxy resin via wire electrode heating [14]. This approach not only reduces wire breakage but also increases cutting speed and improves surface quality [15]. Additionally, a sandwich technique assisted by titanium (Ti) was employed and enabled the production of polymer composite materials with complex surface profiles [16, 17]. Another technique for cutting CFRP is high-speed WEDM, which uses reusable reciprocating molybdenum wire. The feasibility of machining 1mm thin CFRP composites using a 2mm sandwich assisting electrode with HS-WEDM was investigated [18]. Also examined the impact of using a 3mm sandwich made of H13 steel and copper foil, as reported by [19]. The results indicated that cutting without sandwich-assisting electrodes led to deviations in the straightness of the cutting profile.

WEDM machining precision is divided into two categories: shape accuracy and precise positioning. Shape accuracy is primarily concerned with corner-machining precision and the straightness of the machined surface. Several factors, including wire vibration, dielectric fluid resistance, process parameters, machining speed, and others, can impact these accuracies. When cutting sharp corners at the tip, there is often a tendency for significant cutting errors to occur due to wire lag and other factors. However, positioning precision is based on both the accuracy of the mechanical movement and the accuracy of the initial positioning [20]. In WEDM, achieving accurate corners can be challenging due to wire breakage, deflection, vibration, and excessive discharge [21–25]. To address this issue, researchers have explored the optimization of process parameters including pulse-on time, pulse-off time, servo voltage, open voltage, wire tension, and dielectric pressure. Changes in the duration of the pulse-on, pulse-off, and discharge gap can have a notable impact on corner inaccuracies and the heat-affected zone [26]. Servo voltage and feed rate were identified as influential parameters, along with dielectric pressure and tension of wire [27]. Various corner angles were examined and highlighted the importance of pulse-on and wire tension in corner inaccuracy [20]. The influence of pulse-on, voltage, and feed rate were emphasized on corner errors in WEDM of Al6061 alloy [28]. Longer pulse-on time and higher discharge peak current lead to increased corner deformation in thin-walled Q235 steel, while longer pulse-off time reduces deformation [29]. An experimental investigation was conducted to examine how major process factors influence the thermal distortion behavior of thin-walled samples made of Inconel 718, AISIH13, and SKD11 materials [30, 31]. The factors influencing sharp corner errors were discussed in thin parts during WEDM [25]. It was observed that increasing pulse-on and pulse-off time increased corner inaccuracy, and

increased wire feed improved corner inaccuracy for triangular cut profiles in aluminum composite mold material [32]. In other studies, [33, 34] they investigated the influence of process parameters and dielectric fluid conductivity on corner error and suggesting that low-conductivity dielectric fluid and optimized process parameters can minimize corner error and improve machining accuracy. Enhancing corner precision was achieved by managing jet flushing and implementing a corner compensation algorithm to modify the wire trajectory according to wire bending and lag [35]. A mathematical model was developed to calculate wire deflection and total machining error, considering the impacts of wire deflection, wire lag, and high discharge on corner precision [36]. A method for elliptic fitting was suggested to characterize the trajectory of the wire electrode center and the model validity was confirmed by assessing corner error at various angles [22]. Two practical approaches were proposed for enhancing corner accuracy in WEDM [37]. These methods involve adjusting the process parameters and adjusting the programmed wire trajectory. A trim-cutting strategy that can reduce corner errors by up to 97% [38]. This strategy includes a second cut with low-energy pulses and a suitable wire offset to remove any uncut material left by the initial rough cut. The study by [39, 40] investigates the use of a path modification strategy to improve corner accuracy in Monel 400 alloy and AISI D3 tool steel. They find that this strategy successfully improves corner accuracy. Another innovative technique is the powder mixed dielectric (PMD) technique, where abrasive powder particles are added to the dielectric fluid to enhance machining performance [41]. The effects of different types and concentrations of powder were examined on the corner accuracy of Ti6Al4V plates with a rectangular profile [42].

Multi-response optimization techniques are ways to determine the best configurations for process variables that impact many quality characteristics. These techniques help raise the effectiveness and performance of machining processes. Weightage principal component analysis (WPCA) in conjunction with GRA was used to optimize the four EDM process variables to minimize SR and maximize MRR for Inconel X-750 [43]. The optimization of milling parameters for graphene oxide-doped epoxy/CFRP composite was achieved through a novel hybridization technique that integrated CoCoSo and PCA [44]. To rank experiment data and determine the ideal parametric combination, the TOPSIS approach was also applied. RSM was utilized to generate experimental data to investigate the influence of four process factors included P_{on}, P_{off}, I, and wire feed on four performance measures MRR, kerf width, SR, and dimensional accuracy of created holes in Inconel 718 using WEDM [45]. Also, Desirability Function Approach (DFA) was applied to identify the optimal combination of the process factors. Six WEDM process parameters for aluminum metal matrix composite (Al/SiC p-MMC) were optimized using DFA [46]. The goal was to reduce the SR and increase the cutting speed. Additionally, it carried out studies utilizing a Box-Behnken design and fitted responses using quadratic regression models. Prediction models and use RSM and GA to optimize graphene oxide/CF machining performance. It considers various drilling parameters affecting the SR and thrust force of the drilled holes, including spindle speed, feed rate, diameter, and nanofiller content [47].

Based on the previous literature review, there exists a research gap concerning the investigation and optimization of machining sharp corners in thin-walled CFRP using HS-WEDM. This research seeks to study the influence of varied process parameters such as pulse-on, pulse-off duration, and input current, in conjunction with the thickness of CFRP plates, on corner inaccuracy in thin-walled CFRP composites. Furthermore, the study includes single- and multi-response analyses to optimize the process parameters of HS-WEDM. Experiments were carried out at four distinct corner angles: 30°, 60°, 90°, and 120° to validate the outcomes.

2 Experimentation

This section illustrates the material, experimental design, equipment and instruments, and the quantitative data acquisition procedures to provide the study objectives. According to the manufacturing company, Shenzhen Sunlike Electronics Co., Ltd., China manufactured the 3K CFRP composite utilized in this investigation [48], with a fiber volume proportion of approximately 60%. Table 1 illustrates the characteristics of the SYT45 3K CFRP composite used in this study. The 3K CFRP composite material samples were made by stacking layer upon layer of 0°/90° woven carbon fiber and epoxy resin to achieve the appropriate thickness. 3K denotes that each bundle contains 3000 filaments of carbon fiber. The samples were fabricated by applying pressure to the CFRP layers at a temperature of 125 °C in a cavity with an internal heater. The curing process lasted for 180 min and a forming pressure of 5 kg/cm² was applied. A schematic diagram of the preparation procedure of the CFRP composite was illustrated in Fig. 1. The study utilized four flat matte sheet workpieces measuring 75×125mm each. These workpieces featured carbon fiber orientations of (0°/90°) with varied thicknesses of 0.5, 1.0, 1.5, and 2.0 mm.

Table 1 Properties of CFRP used in the study

Material type: SYT45 3K carbon fiber			
Testing items	Testing standard	Scope Of control	Detection result
Linear density(g/km)	GB/T3362-2005	192–204	197
Density (g/cm)	GB/T3362-2005	1.78–1.82	1.79
Tensile strength (MPs)	GB/T3362-2005	≥4000	4098
Intensity Cv (%)	GB/T3362-2005	≤6.0	5.2
Modulus (GPa)	GB/T3362-2005	230–250	236
Elongation (%)	GB/T3362-2005	≥1.5	1.7
Glue ratio (%)	GB/T26752-2011	0.6–0.8	0.7

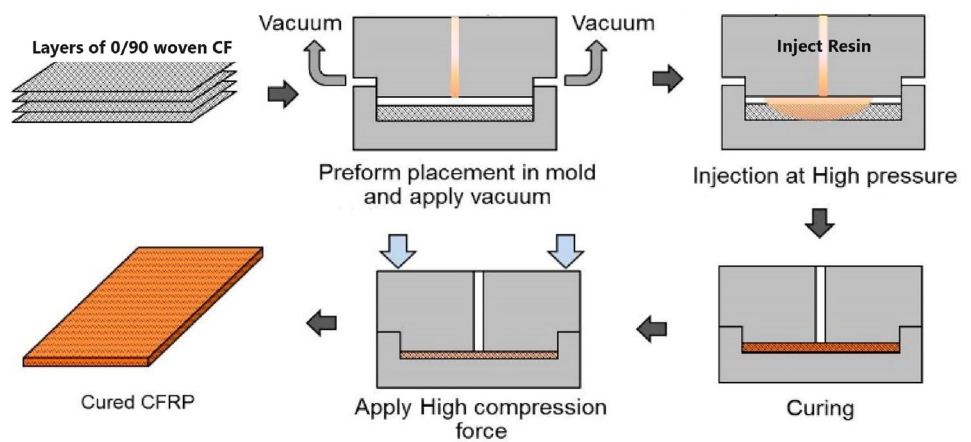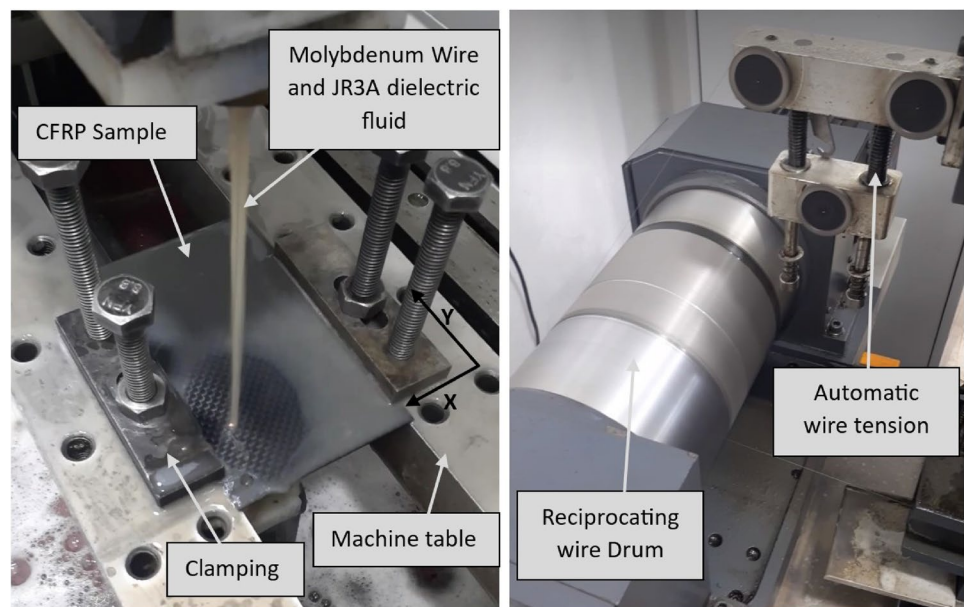**Fig. 1** Schematic diagram of the preparation procedure of CFRP composite

Fig. 2 Experimental setup for cutting thin CFRP plate

Esuntek EFH43F with CNC controller system model EFH-CC2.0 setup was used to cut thin CFRP plates, as shown in Fig. 2. Some of the features and specifications of the EFH43F model are surface finish: 1.0μm, machining precision: 0.012mm, cutting speed: Max = 180 mm²/min, largest workpiece size: 760 × 560 × 300mm, XYZ axle travel: 400 × 350 × 250 mm, cutting taper: Max = ± 3°/80mm, and electrode wire size: Φ0.13-Φ0.20mm. A schematic diagram of the reciprocating WEDM was illustrated in Fig. 3. AutoCAD software was used to design the cutting shape. The
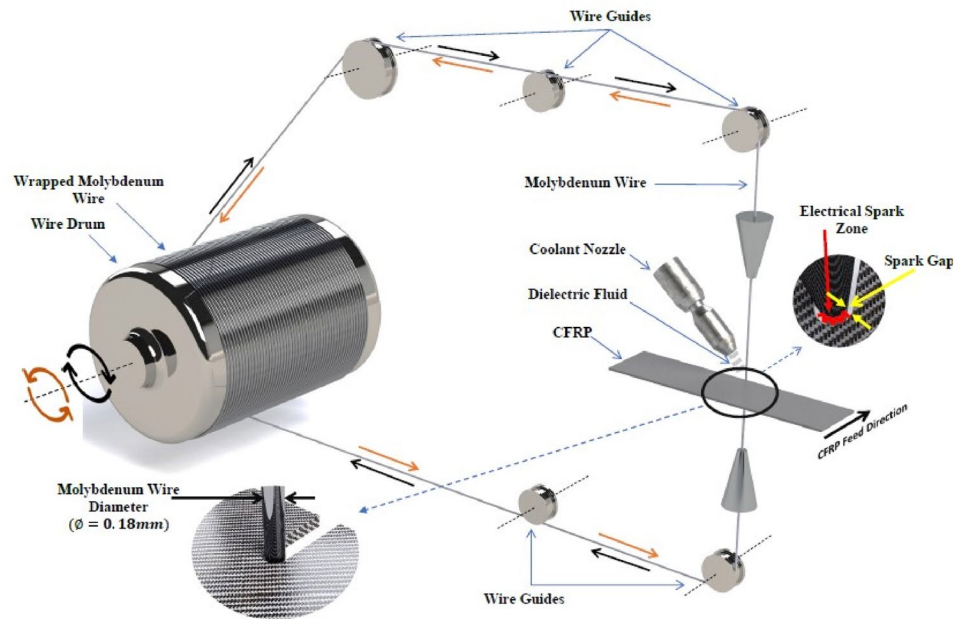
Fig. 3 Schematic diagram of HS-WEDM

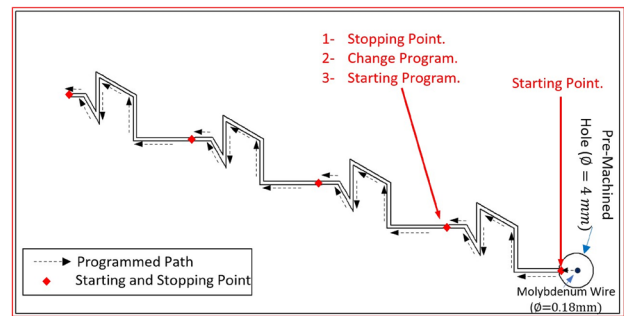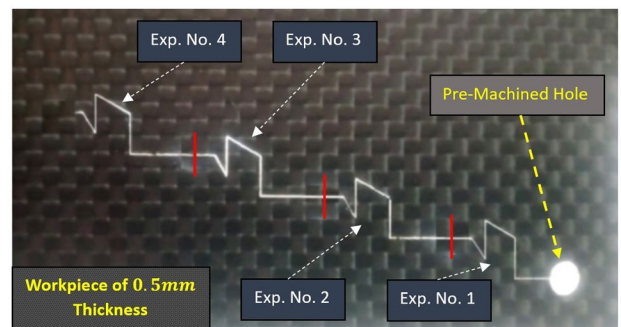**Fig. 4** Schematic diagram for programmed wire trajectory of the four experiments in each workpiece

Fig. 5 Machined workpiece

experiment involved machining four corners with angles of 30°, 60°, 90°, and 120°, as shown in Figs. 4 and 5. The corner characteristic such as corner inaccuracy was considered as a response. The molybdenum cutting wire was inserted through a previously machined hole, which served as the starting point for the experiment. The machine table moved in the X and Y directions, following the specified program path, until all straight lines and corners of the first workpiece with a thickness of 0.5 mm were machined. The program then paused briefly to modify the setting parameters for the next experiment (experiment # two) on the same workpiece. This process was repeated four times for each workpiece.

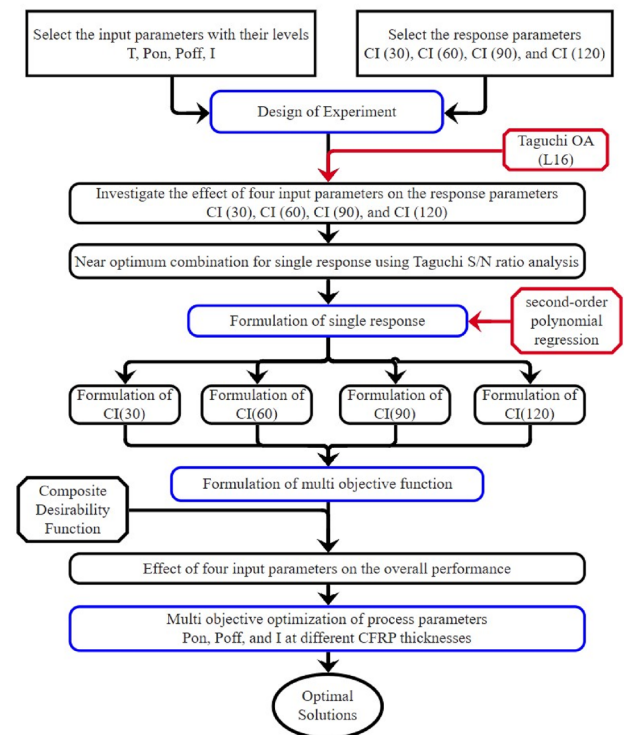○ Discover

Fig. 6 Experimentation methodology flow chart

Table 2 Taguchi L_{16} orthogonal array

Exp. no	$T(mm)$	$P_{on}(\mu s)$	$P_{off}(\mu s)$	$I(A)$	Exp. no	$T(mm)$	$P_{on}(\mu s)$	$P_{off}(\mu s)$	$I(A)$
1	0.5	30	15	2	9	1.5	30	25	5
2	0.5	40	20	3	10	1.5	40	30	4
3	0.5	50	25	4	11	1.5	50	15	3
4	0.5	60	30	5	12	1.5	60	20	2
5	1.0	30	20	4	13	2.0	30	30	3
6	1.0	40	15	5	14	2.0	40	25	2
7	1.0	50	30	2	15	2.0	50	20	5
8	1.0	60	25	3	16	2.0	60	15	4

The optical OPTIKA microscope B600-MET ITALY was used in this study. The lens used to magnify the machined samples is LM Plain (10X/0.3). The microscope's camera captures images of each corner, which are then stored on an external memory card. Measurements on these images are performed using a specialized program called OPTIKA Vision. This program is an accessory provided by the same manufacturer of the microscope.

The process of preparing and carrying out experiments to test a hypothesis and get reliable results is known as the experimental design technique. Taguchi methodology was used in this work. The approach utilized for performing experiments, evaluating the outcomes, and optimization is illustrated in Fig. 6 through a flowchart. The most essential and influenced controllable factors that were considered in this work are P_{on}, P_{off}, I, and CFRP plate thickness (T). Each controllable factor has 4 levels. The specific Taguchi orthogonal array (OA) chosen from the standard OA is L_{16}. The selected controllable parameters and their values that will be used in the experiment were chosen after reviewing some studies on HS-WEDM of CFRP that had been recognized. The following factors were kept constant throughout the tests: voltage is equal to 60 Volt, the head height is 220 mm, the max wire feed is 80 mm²/min, wire speed is (4 m/sec) coded in a machine is 2, molybdenum wire, diameter of wire ($\varnothing = 0.18$ mm), and the JR3A dielectric was mixed with water at the ratio of (1:40 ~ 50). Based on this, a total of 16 experiments were conducted, each with a unique combination of parameter levels, as shown in Table 2.

The corner inaccuracy (CI) refers to the area that remains uncut or overcut between the actual profile and the desired programmed profile as shown in Fig. 7. Corner inaccuracy, or corner error, is an important factor in the
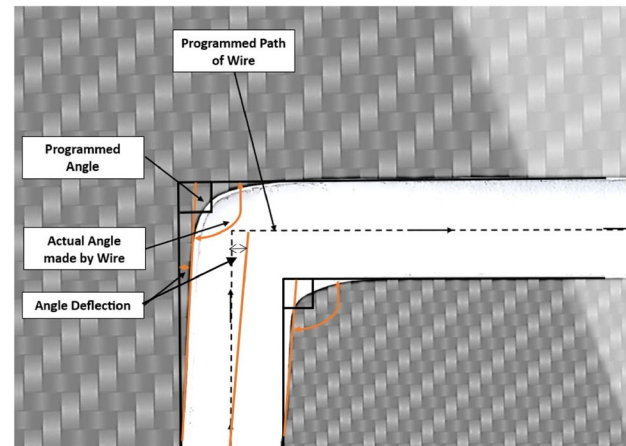
Fig. 7 Schematic diagram of corner inaccuracy

Fig. 8 Sample of area *CI* measurement 30° and 60°
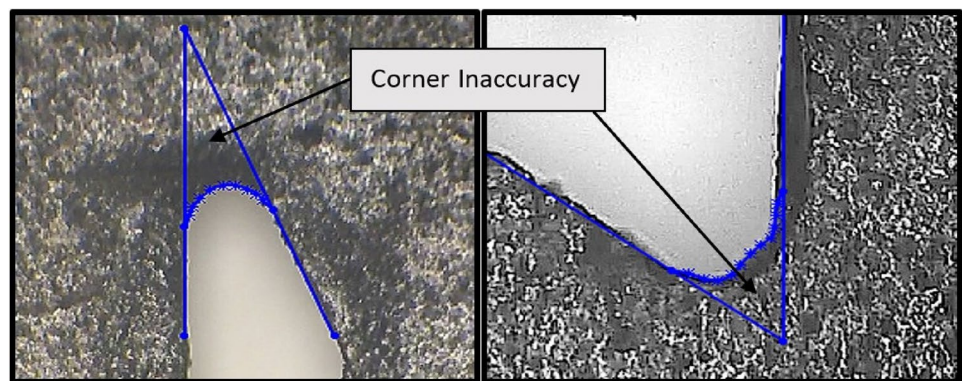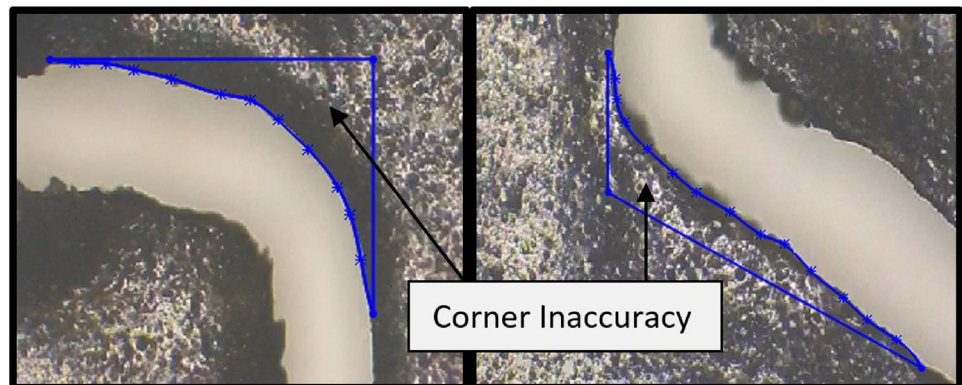

Fig. 9 Sample of area *CI* measurement 90° and 120°

HS-WEDM process when machining complex shapes. In this study, the outside corner inaccuracy angle refers to the inaccuracy that occurs when producing an interior shape in a CFRP sheet. Measurements of the corner inaccuracy in the sample area are shown in Figs. 8 and 9. To measure the corner inaccuracy area, images were captured using the Optika microscope and saved on external storage. The Optika Vision software was then used to place a real scale on the image. The image was then imported into SolidWorks software, where the actual angle was placed on the image and the corner inaccuracy area was measured. Table 3 presents the measurements of the corner inaccuracy for four different angles: 30°, 60°, 90°, and 120°.

Table 3 Measurements of the corner inaccuracy for different angles: 30°, 60°, 90°, and 120°

Exp.no	Corner Inaccuracy $(CI)(mm^2)$				Exp. no	Corner Inaccuracy $(CI)(mm^2)$			
	$CI_{30°}$	$CI_{60°}$	$CI_{90°}$	$CI_{120°}$		$CI_{30°}$	$CI_{60°}$	$CI_{90°}$	$CI_{120°}$
1	0.0704	0.0661	0.0566	0.0880	9	0.1257	0.0982	0.0635	0.1810
2	**0.0334**	0.0690	0.0253	0.0581	10	0.1082	0.0774	0.0480	0.0870
3	0.1330	0.0489	0.1224	0.1789	11	0.1131	0.1222	0.0385	0.0446
4	0.1391	0.1950	0.2606	0.1974	12	0.2074	0.1130	0.0533	0.0451
5	0.0633	0.0643	0.0913	0.1161	13	0.1170	0.1170	0.0473	0.1335
6	0.0633	0.0386	0.0137	**0.0196**	14	0.0972	0.1200	0.0459	0.1410
7	0.0725	0.0728	**0.0124**	0.0355	15	0.2100	0.2000	0.1800	0.1900
8	0.1375	**0.0300**	0.0205	0.0220	16	0.2177	0.2073	0.1771	0.1407

Bold numbers represent the best value obtained from the experiments for each corner angle

3 Results and discussion

This section investigates and discusses the factors that influenced the corner characteristics. The Taguchi approach for single-response optimization and desirability function approach for multi-response were also examined and discussed. The data used in this section was illustrated in the previous Table 3. WEDM, like many other machining methods, cannot produce extremely sharp corners. The corner inaccuracy is affected by numerous parameters, including T, P_{on}, P_{off}, I, and wire electrode diameter (d_w). Furthermore, the minimal size of the CI is affected by the angle of the corner, i.e., the amount of the dihedral angle created between each pair of adjacent machined surfaces. Note that, when the wire completes its intended trajectory without encountering any problems that prevent it from completing the path (perfectly machining), it should have the minimum CI. Consequently, as shown in Fig. 10, the minimum CI differs for angles 30°, 60°, 90°, and 120°. Furthermore, the largest minimum corner inaccuracy area (CI_{Min}) was achieved at the smallest corner angle (i.e., $CI_{min_{30°}} > CI_{min_{60°}} > CI_{min_{90°}} > CI_{min_{120°}}$). Based on geometrical calculation (using SolidWorks) for each angle, at diameter of the wire ($\phi = 0.18$ mm), and average gap produced by the process parameters ($S = 20 \sim 25$ μm), the rest material of the corners is 0.02423mm², 0.00685mm², 0.0021mm², and 0.000538mm² for $CI_{30}°$, $CI_{60}°$, $CI_{90}°$, and $CI_{120}°$, respectively. The minimum corner radius can be performed as follows:

$$R_{Min} \geq S + \left(\frac{d_w}{2} \right)$$

where S is the gap wire (overcut) and d_w is the wire diameter (0.18 mm).

3.1 Effect of process parameters and CFRP thickness

Figures 11 and 12 display the main effect plot showing the impact of pulse-on duration and input current on corner inaccuracy (CI) across various corner angles (30°, 60°, 90°, and 120°). The results demonstrate that the corner inaccuracy initially decreases with an increase in pulse-on duration from 30μs to 40μs and input current from 2 to 3A. However, as both pulse-on duration and input current continue to increase, the corner inaccuracy subsequently increases.

Generally, the duration and intensity of discharge energy are influenced by the pulse-on duration and input current. Consequently, elevating the pulse-on duration and current leads to higher discharge energy, resulting in increased material removal due to the generation of intense heat. Also, it is affecting the wire vibration, which is the oscillation of the wire due to electrodynamic forces and thermal expansion. The wire vibration can cause the wire to deviate from the desired path and result in corner errors and angular errors [49, 50].

However, this study discovered that as the discharge energy rises due to increase in pulse-on (more than 40μs) and current (more than 3A), there is an increase in the amount of debris particles (matrix and carbon fiber evaporated) generated in the machining gap zone due to enhanced material removal. Some of these particles possibly solidify and accumulate (recast layer) in the machined gap area. The effect of the recast layer on the corner accuracy depends on the thickness of layer, hardness, and morphology. Consequently, a portion of the discharge energy is utilized to re-melt and vaporize these accumulated debris particles and recast layer, which reduces the actual energy that evaporates the raw material. This possibly increases wire deflection and vibration during machining, altering the effective gap width, and causing irregular discharge, which affects the corner accuracy [20, 26].
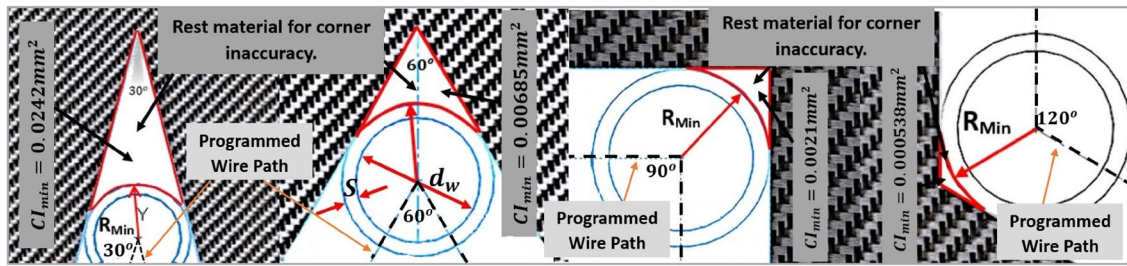
Fig. 10 Corners inaccuracy area for perfect machining of various corner angles 30°, 60°, 90°, and 120°

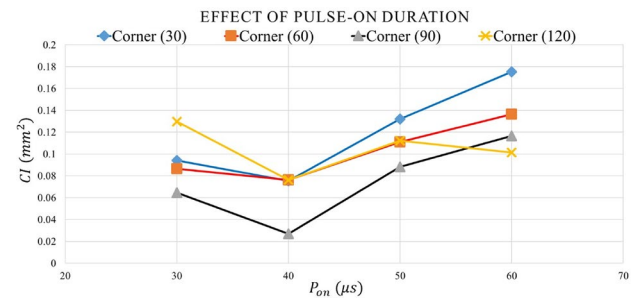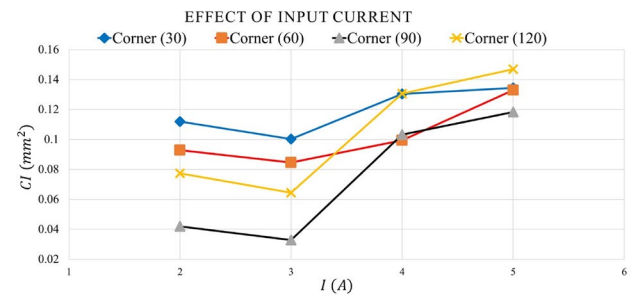**Fig. 11** Effect of pulse-on duration (P_{on}) on the CI of different corner angles

Fig. 12 Effect of input current (I) on the CI of different corner angles

Wire deflection in WEDM is a phenomenon that impacts the precision and quality of the finished components. Wire deflection, also known as wire lag, occurs when the wire electrode bends or strays from its intended trajectory due to the forces applied by sparks, wire tension, and dielectric fluid. This deviation can lead to inaccuracies in the shape and dimensions of the workpiece, particularly in corners and curved sections. Various factors, including wire diameter, material of wire, feed rate, spark gap, input current, pulse duration, voltage, dielectric type, dielectric flow rate, and characteristics of the workpiece material, and thickness, can influence wire deflection [51–53].

The duration of the pulse-off period in WEDM denotes the time elapsed between current pulses. This duration influences the cooling and flushing effects of the dielectric fluid on both the wire and the CFRP plate. A shorter pulse-off duration results in more discharges occurring within a specific time, consequently increasing the material removal rate. Conversely, extending the pulse-off duration enhances dimensional accuracy by diminishing wire deflection and slowing the cutting speed [54–56]. This also results in more dispersed sparks. In Fig. 13, it can be seen that a high pulse-off duration at 25 ~ 30μs improves *CI* at corner angles of 30°, 60°, and 90°. However, for a corner angle of 120°, a lower pulse-off duration of 15μs achieved the best corner accuracy.

As illustrated in Fig. 14, at a thickness of 0.5mm, excessive thermal deformation occurred due to excessive discharge at the thin wall (i.e., the small cross-section area of the specimen in which the charge is concentrated), resulting in increased error at the corner. Increasing the thickness of the CFRP to 1.0mm resulted in an enhancement of corner precision due to a larger exposed area to the discharge energy. However, increasing the CFRP plate thickness beyond 1.0mm led to a rise in corner inaccuracies, likely because of the expanded cut cross-section area, causing more matrix and fibers to evaporate during machining. This causes the wire to deviate from the desired path and result in corner errors and angular errors [57, 58].

Discover

Fig. 13 Effect of pulse-off duration (P_{off}) on the CI of different corner angles
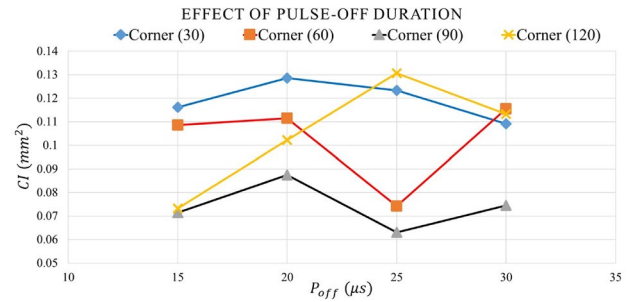

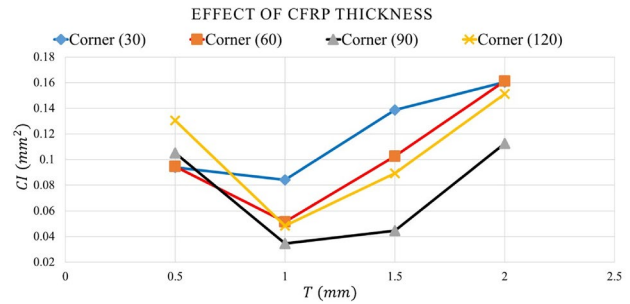**Fig. 14** Effect of CFRP thickness (T) on the CI of different corner angles

Table 4 Taguchi responses tables for corner inaccuracy for different angles

Response Table for S/N Ratios (Smaller is better)

Level	$T(mm)$	$CI_{30°}$			$T(mm)$	$CI_{60°}$		
		$P_{on}(\mu s)$	$P_{off}(\mu s)$	$I(A)$		$P_{on}(\mu s)$	$P_{off}(\mu s)$	$I(A)$
1	21.81	20.92	19.80	19.94	21.81	21.56	20.95	20.93
2	**21.99**	**23.26**	**20.18**	**21.08**	**26.33**	**23.03**	20.00	**22.65**
3	17.48	18.20	18.25	18.51	19.90	20.30	**23.81**	21.49
4	16.42	15.32	19.47	18.17	16.17	19.32	19.46	19.15
Delta	5.57	7.95	1.93	2.91	10.15	3.72	4.36	3.49
PCR%	30.34	43.30	10.51	15.85	46.73	17.13	20.07	16.07
Rank	2	1	4	3	1	3	2	4
Level	T(mm)	$CI_{90°}$			T(mm)	$CI_{120°}$		
		$P_{on}(\mu s)$	$P_{off}(\mu s)$	$I(A)$		$P_{on}(\mu s)$	$P_{off}(\mu s)$	$I(A)$
1	22.11	24.05	26.38	28.83	18.72	18.04	**24.83**	23.51
2	**32.49**	**32.23**	23.27	**30.12**	**28.75**	**24.28**	21.19	**25.59**
3	27.66	24.89	25.68	21.76	22.50	21.35	19.99	17.97
4	20.80	21.89	**27.73**	22.35	16.49	22.80	20.45	19.38
Delta	11.69	10.34	4.45	8.37	12.26	6.24	4.84	7.62
PCR%	33.54	29.67	12.77	24.02	39.60	20.16	15.63	24.61
Rank	1	2	4	3	1	3	4	2

Bold numbers represented the maximum S/N ratio values for each factor. These bold numbers are used to identify the optimum combination levels for each factor

The orientation of the fibers is of crucial importance for the material removal mechanism of CFRP composites during the WEDM process. These composites are typically bi- or multi-directional and are used in a wide variety of applications. Maintaining consistent cutting directions with fiber orientations can be a significant challenge when cutting complex shapes or corners in CFRP composites with unidirectional, multidirectional, or bidirectional carbon fibers. Changes in cutting direction

based on fiber orientations can have either positive or negative effects on the cutting mechanism. For the purpose of this study, CFRP samples containing 0°/90° woven carbon fibres have been used. As shown in Fig. 5, the cutting process was designed to ensure that one of the two kerfs (kerfs that form a corner) was always oriented either vertically or horizontally. For corners of 30°, 60° and 120°, the other kerf is inclined at 30°/60° relative to the carbon fiber direction. This minimises the effect of changing cutting directions on these corners. The two cuts forming a 90° corner are parallel and perpendicular to the carbon direction.

3.2 Single response analysis

Taguchi analysis was used to obtain the near optimum combination from the visible parameter levels. Based on the analysis of the Taguchi S/N ratio of corner inaccuracy that illustrated in Table 4, the Percentage Contribution Ratio (PCR) indicates that the most influential process parameters are as follows: P_{on} (PCR = 43.3%), P_{off} (PCR = 20.07%), P_{on} (PCR = 29.67%), and input current (PCR = 24.61%) for angles 30°, 60°, 90°, and 120°, respectively. Also, CFRP thickness has the most significant impact on the corner inaccuracy, which has PCR equal to 30.34%, 46.73%, 33.54%, and 39.60% for corner angles 30°, 60°, 90°, and 120°, respectively. The PCR measures the ratio of factor delta to the total delta of all factors. Table 4 also illustrates the importance of the input parameters by ranking them. In addition, Fig. 15 illustrates the near optimum combinations resulting from Taguchi analysis for minimizing the corner inaccuracy. As indicated by the bold type in Table 4, the Taguchi optimal combination is determined from the maximum S/N ratio values of factor level. These combinations are not included in the OA that was illustrated in Table 2, so the predicted value (Taguchi) test of these combinations was processed. The predicted (calculated) value (Taguchi) of CI using the near-optimum combination can be calculated from Eq. (1).

$$\eta_{pred} = \eta_m + \sum_{i=1}^{n}(\eta_i - \eta_m) \tag{1}$$

where η_m is the total mean S/N, $\sum_{i=1}^{n}(\eta_i - \eta_m)$ is all improvement (contribution) from all, η_i is the mean S/N for factors at designated optimal levels, and n is the number of the main factors that affect the quality characteristics. As depicted in Fig. 15, the result of the predicted Taguchi values for the near optimum combinations (NOC) of CI for different corner angles were compared with the best CI values estimated from Table 3 (corner inaccuracy measurements).

3.3 Multi-response optimization

3.3.1 Modeling of CI using second-order polynomial regression

The polynomial regression models describe the correlation between p input variables $x_1, \ldots, x_p$ and a single output variable y as illustrated in Eq. (2) [59].

$$y = \beta_0 + \sum_{j=1}^{p} \beta_j x_j + \sum_{j<k} \beta_{jk} x_j x_k + \sum_{j=1}^{p} \beta_{jj} x_j^2 + \varepsilon \tag{2}$$

where β_0 is an intercept, and β_j, β_{jk}, and β_{jj} are regression coefficients related to the main effect, relations effect, and quadratic effect terms, respectively; in Eq. (2), the number of regression coefficients to be estimated by "p'= 1 + 2p + p(p-1)/2", ε includes various sources of errors such as error of measurement for the dependent variable y, errors in specifying regression functions, and errors from excluding other input variables. The 2nd order polynomial modeling was implemented using Minitab software package V21.1 under consideration of forward information criteria with hierarchical model for the data shown in Table 3. The response equations were formulated for the CI of angles 30°, 60°, 90°, and 120°, as illustrated in Equs. (3, 4, 5, and 6). In this test, the adequacy measure R^2 was suggested that the models were adequate and fit. The R^2 values for $CI_{30}{}^{o}$, $CI_{60}{}^{o}$, $CI_{90}{}^{o}$, and $CI_{120}{}^{o}$ are 87.36%, 91.73%, 93.10%, and 94.03%, respectively. Figure 16 depicts the actual value of responses and the predicted values estimated from the model to demonstrate the validity of these models. The average error of the models was estimated from the ANOVA for $CI_{30}{}^{o}$, $CI_{60}{}^{o}$, $CI_{90}{}^{o}$, and $CI_{120}{}^{o}$ are 12.64%, 8.27%, 6.90%, and 5.97%, respectively, as shown in Tables 5 and 6. Also, F-values and contribution for model parameters were established.
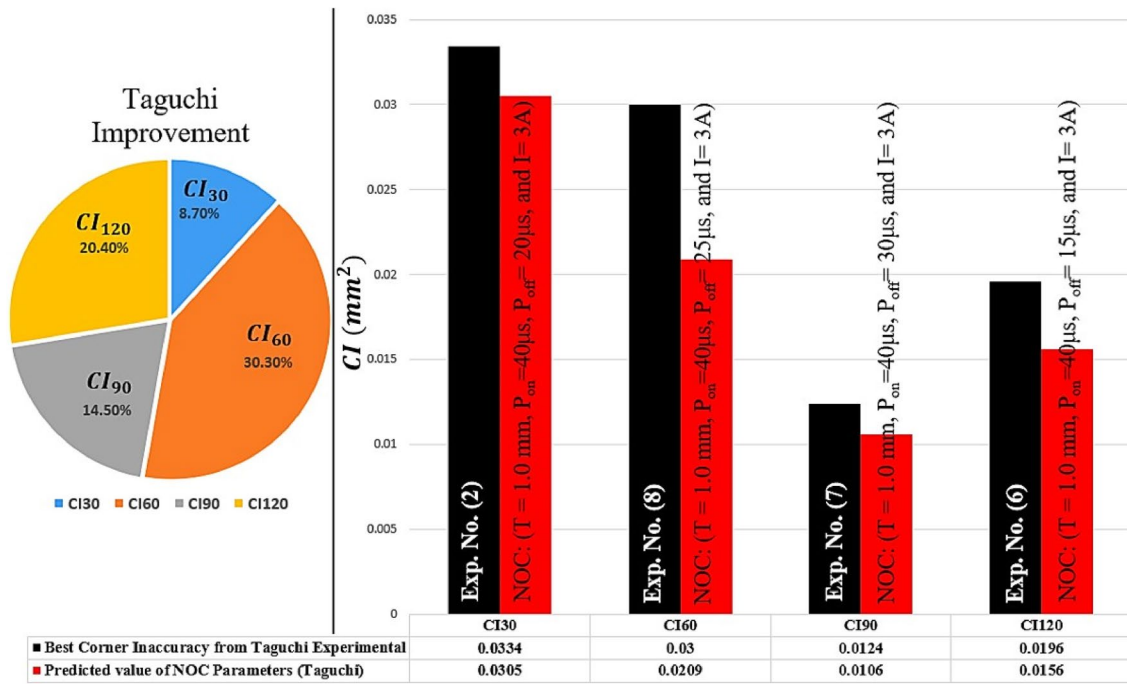
Fig. 15 *CI* for Taguchi predicted values Vs best *CI* estimated from Taguchi experimental design
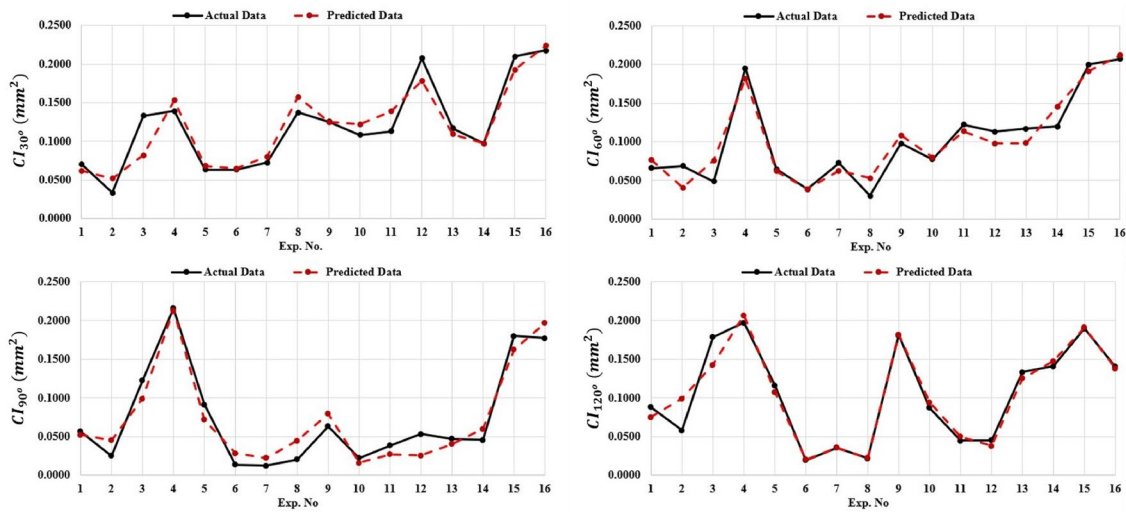

Fig. 16 The predicted values versus the experimental values for corner inaccuracy responses of the mathematical model

$$
\begin{aligned}
CI_{30^\circ} = {} & 0.289 + (0.0044 * T) - (0.00643 * P_{on}) - (0.00663 * P_{off}) \\
& - (0.0528 * I) + (0.000107 * P_{on}^2) \\
& + (0.0155 * T * I) + (0.00192 * P_{off} * I)
\end{aligned}
\tag{3}
$$

Table 5 ANOVA of corner inaccuracy models of corner angles 30° and 60°

ANOVA of $CI_{30°}$			ANOVA of $CI_{60°}$		
Source	Contribution (%)	F-Value	Source	Contribution (%)	F-Value
Linear	72.59	12.43	Linear	48.27	4.13
T	28.35	20.17	T	26.26	15.92
Pon	39.71	26.77	Pon	14.27	0.17
Poff	0.30	0.01	Poff	0.11	0
I	4.24	2.68	I	7.62	0.1
Square	8.41	2.06	Square	28.00	0.92
Pon*Pon	8.41	2.06	T*T	21.68	0.78
2-Way Interaction	6.37	2.02	Pon*Pon	2.64	0.19
T*I	2.76	1.75	I*I	3.68	1.78
Poff*I	3.61	2.29	2-Way Interaction	15.46	1.87
Error	12.64		T*Pon	0.72	0.01
Total	100.00		T*Poff	8.01	3.87
			Pon*I	3.33	0.96
			Poff*I	3.40	1.64
			Error	8.27	
			Total	100.00	

Table 6 ANOVA of corner inaccuracy models of corner angles 90° and 120°

ANOVA of $CI_{90°}$			ANOVA of $CI_{120°}$		
Source	Contribution (%)	F-Value	Source	Contribution (%)	F-Value
Linear	43.45	2.48	Linear	37.21	11.14
T	0.33	1.68	T	3.58	7.49
Pon	14.90	0.2	Pon	0.81	10.02
Poff	0.07	0.15	Poff	7.44	7.47
I	28.15	4.45	I	25.38	4.55
Square	37.16	5.33	Square	39.94	10.74
T*T	30.26	5.65	T*T	34.88	27.15
Pon*Pon	6.90	5	Poff*Poff	3.62	3.64
2-Way Interaction	12.50	2.27	I*I	1.43	1.44
T*Pon	2.10	0.39	2-Way Interaction	16.88	8.48
T*Poff	7.93	5.75	T*Poff	9.82	9.86
Pon*Poff	2.46	1.21	Poff*I	7.06	7.09
Pon*I	0.01	0.01	Error	5.97	
Error	6.90		Total	100.00	
Total	100.00				

$$
\begin{aligned}
CI_{60°} = \ & 0.332 + (0.175 * T) - (0.00818 * P_{on}) \\
& + (0.00631 * P_{off}) - (0.1650 * I) + (0.0477 * T^2) \\
& + (0.000039 * P_{on}^2) + (0.01048 * I^2) \\
& + (0.00023 * T * P_{on}) - (0.01076 * T * P_{off}) \\
& + (0.00110 * P_{on} * I) + (0.00201 * P_{off} * I)
\end{aligned}
\tag{4}
$$

Table 7 Range of Input Variables and Responses for corner inaccuracy of angles 30°, 60°, 90°, 120° Simultaneously

Response	Goal	Lower	Target	Upper	Weight
$CI_{30°}(mm^2)$	Minimize	0.0196	0.0196	0.197413	1
$CI_{60°}(mm^2)$	Minimize	0.0124	0.0124	0.216	1
$CI_{90°}(mm^2)$	Minimize	0.03	0.03	0.207334	1
$CI_{120°}(mm^2)$	Minimize	0.0334	0.0334	0.217701	1
	Parameters			Parameters Ranges	
	CFRP Thickness (T)			Hold at the thickness to be cut	
	Pulse-on Duration (P_{on})			30µs up to 60µs	
	Pulse-off Duration (P_{off})			15µs up to 30µs	
	Input Current (I)			2A up to 5A, with step 1A	

Table 8 Composite desirability for the overall responses based on Taguchi OA

Exp. No	$CI_{30°}(mm^2)$	$CI_{60°}(mm^2)$	$CI_{90°}(mm^2)$	$CI_{120°}(mm^2)$	Composite Desirability (CD) value
1	0.0704	0.0661	0.0566	0.0880	0.7658
2	0.0334	0.0690	0.0253	0.0581	**0.7904**
3	0.1330	0.0489	0.1224	0.1789	0.5555
4	0.1391	0.1950	0.2160	0.1974	0.0000
5	0.0633	0.0643	0.0913	0.1161	0.6972
6	0.0633	0.0386	0.0137	0.0196	**0.9219**
7	0.0725	0.0728	0.0124	0.0355	0.8525
8	0.1375	0.0300	0.0205	0.0220	0.6961
9	0.1257	0.0982	0.0635	0.1810	0.3557
10	0.1082	0.0774	0.0225	0.0870	**0.6785**
11	0.1131	0.1222	0.0385	0.0446	0.6463
12	0.2074	0.1130	0.0533	0.0451	0.5760
13	0.1170	0.1170	0.0473	0.1335	**0.5964**
14	0.0972	0.1200	0.0459	0.1410	0.4685
15	0.2100	0.2000	0.1800	0.1900	0.1019
16	0.2177	0.2073	0.1771	0.1407	0.0000

Bold numbers represented the best experiment that has max composite desirability values at each CFRP thickness (0.5, 1.0, 1.5, 2.0mm)

$$CI_{90°} = 0.464 - (0.089 * T) - (0.02332 * P_{on}) + (0.0048 * P_{off})$$
$$+ (0.0145 * I) + (0.1348 * T^2) + (0.000166 * P_{on}^2)$$
$$+ (0.00135 * T * P_{on}) - (0.01236 * T * P_{off})$$
$$+ (0.000257 * P_{on} * P_{off}) + (0.00010 * P_{on} * I)$$
(5)

$$CI_{120°} = -0.018 - (0.002 * T) - (0.00340 * P_{on})$$
$$+ (0.0301 * P_{off}) - (0.1005 * I) + (0.1299 * T^2)$$
$$- (0.000465 * P_{off}^2) + (0.00730 * I^2)$$
$$- (0.01293 * T * P_{off}) + (0.00284 * P_{off} * I)$$
(6)

3.3.2 Composite desirability method

The Taguchi method does not guarantee reaching the optimal solution, but rather seeks to find a solution that is near to the optimum for a single response. Moreover, different combinations of the parameters are required to achieve near-optimal
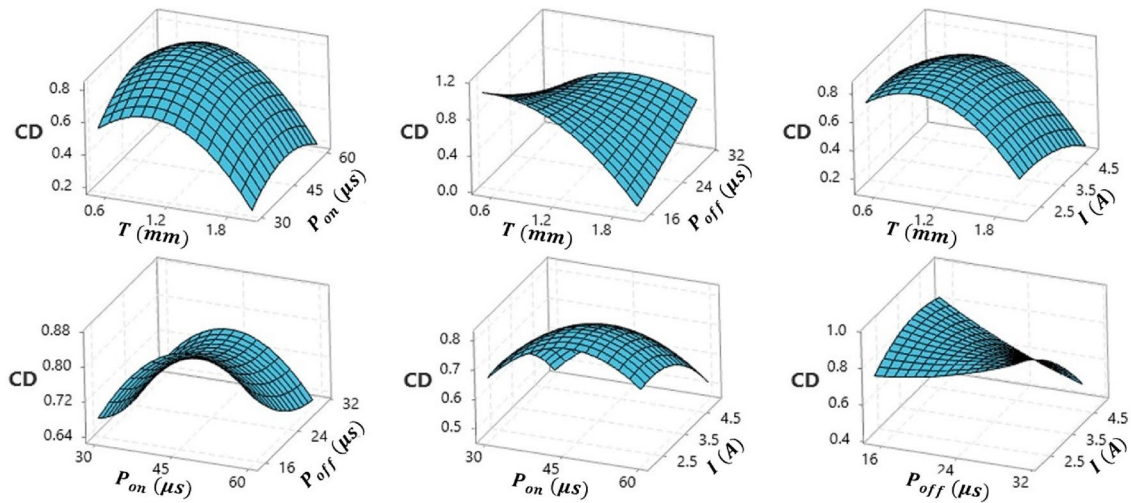
Fig. 17 Effect of process parameters and CFRP thickness on the global composite desirability

conditions for each response. Additionally, the required parameters for making sharp corner angles with high precision for varied CFRP thicknesses cannot be determined. To address this issue of incompatible responses in Taguchi single-response, a multi-response optimization using Composite Desirability (CD) approach coupled with generalized reduced gradient were employed using MINITAB V21.1. The goals and constraints for each response were determined to precisely assess their impact on overall desirability. Table 7 shows the ranges and objectives of the input factors and response characteristics. The global composite desirability for overall responses for the Taguchi OA L_{16} was estimated and illustrated in Table 8. In the first step, individual desirability functions ($d_i(\hat{y}_i)$) must be created for each response ($\hat{y}_i(k)$) using the fitted models and establishing the optimization criteria. Global desirability values range from 0 to 1, where $d_i(\hat{y}_i) = 0$ represents an undesirable response and $d_i(\hat{y}_i) = 1$ represents an ideal response. The Derringer desirability function [60] allows analysts to create different functions based on their optimization criteria. These functions consider an acceptable range of response values, which is determined by the upper (U_i) and lower (L_i) acceptable values. In this study, the goal is to reduce the corner inaccuracy at different angles. The equation for desirability $d_i(\hat{y}_i)$ when it has to be minimized was illustrated by Eq. (7). After transforming the n variables (factor and response levels) into desirability functions, they are combined into a single function called the global Composite Desirability (CD) to determine the best joint responses using Eq. (8). The interaction effect of input parameters P_{on}, P_{off}, I, and T on the overall corner inaccuracy (i.e., composite desirability) was shown in Fig. 17.

$$d_i\left(\hat{y}_i(x)\right) = \begin{bmatrix} 1 & if\ \hat{y}_i(x) < L_i \\ \left(\frac{U_i - \hat{y}_i(x)}{U_i - L_i}\right)^t & if\ L_i \leq \hat{y}_i(x) \leq U_i \\ 0 & if\ \hat{y}_i(x) > U_i \end{bmatrix} \tag{7}$$

$$CD = \left(d_1^{r1} \times d_2^{r2} \cdots \cdots \times d_n^{rn}\right)^{\frac{1}{\Sigma ri}} = \left(\prod_{i=1}^{n} d_i^{ri}\right)^{\frac{1}{\Sigma ri}} \tag{8}$$

where t is the weight to determine how important is it for $\hat{y}_i$ to be close to the minimum, *ri* is the importance of each variable relative to the others.

The goal of optimization is to identify a favorable set of conditions that will meet all objectives. Figure 18 displays the maximum response value, optimal parameter values, and composite desirability values for $CI_{30}{}^o$, $CI_{60}{}^o$, $CI_{90}{}^o$, and $CI_{120}{}^o$ simultaneously at T (1.0mm). Table 9 displays the predicted best process combinations for achieving optimal overall corner accuracy within the specified design space limitations across various CFRP plate thicknesses ranging from 0.5mm to 2.0mm. The optimal process combination for achieving desired responses within a specified CFRP thickness was selected based on the set of conditions with the highest global desirability value, using generalized reduced gradient (GRG) method. This selection aims to demonstrate the sensitivity of process parameters to variations in CFRP plate thickness. Note that, the HS-WEDM machine in this study has input current values are 2, 3, 4, 5A, no values can be selected within these values. The predicted improvement in corner accuracy was expressed as a percentage is shown in Fig. 19.

Fig. 18 Optimal Solution for $CI_{30}{}^o$, $CI_{60}{}^o$, $CI_{90}{}^o$, and $CI_{120}{}^o$ simultaneously at $T = 1.0$mm
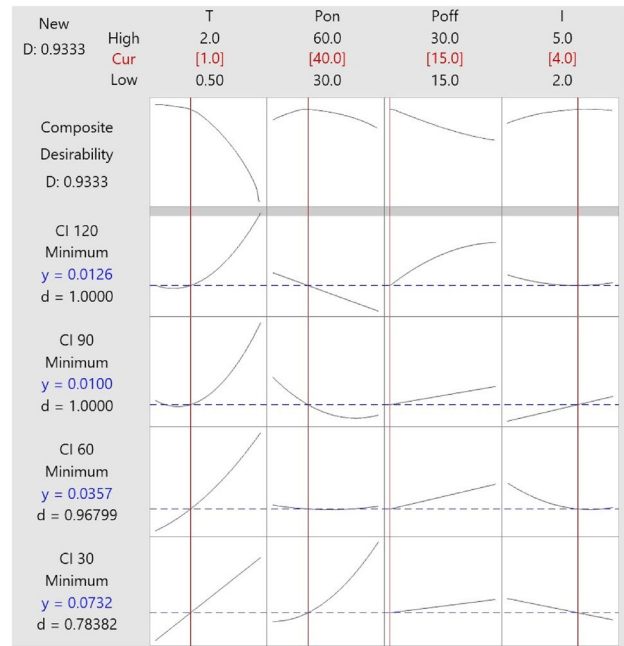
Table 9 Set of Optimal Solutions for $CI_{30}{}^o$, $CI_{60}{}^o$, $CI_{90}{}^o$, and $CI_{120}{}^o$ simultaneously at different thickness

$T(mm)$	Optimal Process Parameters			Corner Inaccuracy				Composite desirability for optimal combination
	$P_{on}(\mu s)$	$P_{off}(\mu s)$	$I(A)$	$CI_{30^o}(mm^2)$	$CI_{60^o}(mm^2)$	$CI_{90^o}(mm^2)$	$CI_{120^o}(mm^2)$	
0.50	41	15	4	0.0447	0.0125	0.0097	0.0062	0.9853
1.00	40	15	4	0.0732	0.0357	0.0100	0.0126	0.9333
1.50	45	30	2	0.0792	0.0637	0.0175	0.0204	0.8823
2.00	45	30	2	0.0968	0.0785	0.0186	0.0529	0.7829
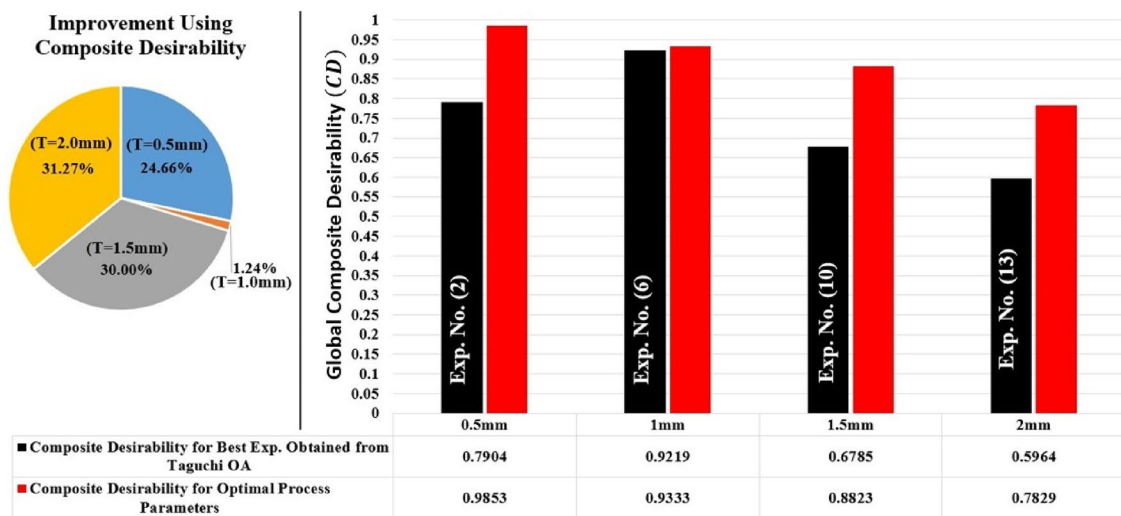
Fig. 19 Improvement using optimal process parameters at varied CFRP thicknesses

This improvement is based on the composite desirability obtained from the optimal process combination presented in Table 9, compared to the composite desirability obtained from the OA experiments shown in Table 8, for different CFRP thicknesses of 0.5, 1.0, 1.5, and 2.0mm.

In order to improve corner accuracy for various CFRP thicknesses, the middle levels of the pulse-on time, which lasts between 40 and 45μs works best, as Table 9 and Fig. 17 show. In addition, thinner CFRP (0.5 to 1.0mm) requires a shortest pulse-off duration, while thicker plates (1.5 to 2.0mm) require a longer duration of pulse-off. For diverse CFRP thicknesses, input currents ranging from 2 to 4A are suitable. Higher input currents necessitate a lower pulse-off time, whereas lower input currents demand a long pulse-off duration to maintain precise corner angles, as depicted in Fig. 17. Notably, at varying input current and pulse-off time levels, the central region of the pulse-on time emerges as crucial for improving corner accuracy. Consequently, certain conflicting process parameters must be reconciled to achieve optimal corner accuracy. The ideal process combination is determined through compromise solutions. Table 9 offers an overview of this optimal combination for varied CFRP thicknesses using GRG optimization method.

4 Conclusions

This work presents, for the first time, an analysis of the corner inaccuracy for the cutting of thin-walled CFRP parts in the corner-cutting step. The fabrication of these parts is challenging work because of its poor stiffness and low electrical conductivity. To address these issues, an investigation of the use of HS-WEDM as a non-contact material removal process that is suitable for machining CFRP composite without the need for a metal-assisted electrode was conducted. A Taguchi analysis allows pointing out the effect of the HS-WEDM process parameters on the corner inaccuracy for the cut of thin-walled CFRP parts in the corner cutting step. Based on our findings, we conclude the following:

The most effective parameters on the corner inaccuracy of angle 30° are pulse-on duration (PCR = 43.3%), followed by CFRP thickness (PCR = 30.34%). Also, CFRP thickness has the greatest influence on corner angles 60°, 90°, and 120° with PCR 46.73%, 33.54%, and 39.6%, respectively. As a result, the most effective parameter influencing corner inaccuracy with varied angles is thickness of CFRP.

Taguchi investigation has identified the near optimum combination for improving corner accuracy at varied corner angles. These combinations consist of T (1mm), P_{on} (40μs), and I (3A) for studied corner angles 30°, 60°, 90°, and 120°. The only factor that changes is the duration of the pulse-off, which is dependent on the corner angle. For a 30° corner angle, a pulse-off duration of 20μs is required, while for angles of 60° and 90°, the pulse-off durations increase to 25μs and 30μs, respectively. As a result, low pulse-off duration is particularly beneficial for small corner angles, as it prevents excessive buildup of debris in machining gap zone.

Composite desirability aims to find the optimal settings for the process parameters that maximize the overall desirability of the corner accuracy for varied angles. Therefore, to achieve accurate corners with different angles of thin walled CFRP, the optimal process parameters were determined: P_{on} (40μs), P_{off} (15μs), and I (4A) for CFRP thicknesses between 0.5 and 1.0mm, and P_{on} (45μs), P_{off} (30μs), and I (2A) for thicknesses between 1.25 and 2.0mm. The improvement occurred from optimization for CFRP thicknesses 0.5, 1.0, 1.5, and 2.0mm are 24.66%, 1.24%, 30%, and 31.27%, respectively.

5 Future work

This study investigates the corner accuracy of thin-walled CFRP composites through the application of an HS-WEDM process without the use of an assisted conductive material. The method effectively machining the CFRP material. Future research could involve examining corner accuracy using HS-WEDM of CFRP composites with varying thicknesses of assisted conductive material (assisted electrode) and comparing the outcomes with those of this study. Given the limited existing research on HS-WEDM of CFRP, further investigation is warranted to analyze how the direction of reciprocating wire motion affects cutting quality.

Data availability The authors confirm that the data supporting the findings of this study is available within the article.

Declarations

Competing interests The authors declare that they have no known competing financial interests or personal relationships that could have appeared to influence the work reported in this paper.

References

1. Khalili S, Daghigh V, Eslami Farsani R. Mechanical behavior of basalt fiber-reinforced and basalt fiber metal laminate composites under tensile and bending loads. J Reinforced Plastics Composites. 2011;30(8):647–59. https://doi.org/10.1177/0731684411398535.
2. Shyha I, Huo D. Advances in Machining of Composite Materials. Cham: Springer; 2021.
3. Geier N, Xu J, Poór DI, Dege JH, Davim JP. A review on advanced cutting tools and technologies for edge trimming of carbon fibre reinforced polymer (CFRP) composites. Compos Part B: Eng. 2023. https://doi.org/10.1016/j.compositesb.2023.111037.
4. Che D, Saxena I, Han P, Guo P, Ehmann KF. Machining of carbon fiber reinforced plastics/polymers: a literature review. J Manuf Sci Eng. 2014;136:3. https://doi.org/10.1115/1.4026526.
5. Ozkan D, Gok MS, Oge M, Karaoglanli AC. Milling behavior analysis of carbon fiber-reinforced polymer (CFRP) composites. Mater Today: Proc. 2019;11:526–33. https://doi.org/10.1016/j.matpr.2019.01.024.
6. Kumar J, Verma RK, Khare P. Chapter THREE - Graphene-functionalized carbon/glass fiber reinforced polymer nanocomposites: fabrication and characterization for manufacturing applications. In: Hussain C, Kumar V, editors. Handbook of Functionalized Nanomaterials. Amsterdam: Elsevier; 2021. p. 57–67.
7. Zhang G, Zhang Z, Guo J, Ming W, Li M, Huang Y. Modeling and optimization of medium-speed WEDM process parameters for machining SKD11. Mater Manuf Processes. 2013;28(10):1124–32. https://doi.org/10.1080/10426914.2013.773024.
8. Mingqi L, Minghui L, Guangyao X. Study on the variations of form and position of the wire electrode in WEDM-HS. Int J Adv Manuf Technol. 2005;25:929–34. https://doi.org/10.1007/s00170-003-1915-4.
9. Oliver Nesa Raj S, Prabhu S. Modeling and analysis of titanium alloy in wire-cut EDM using Grey relation coupled with principle component analysis. Aust J Mech Eng. 2017;15(3):198–209. https://doi.org/10.1080/14484846.2016.1251077.
10. Ghodsiyeh D, Golshan A, Izman S. Multi-objective process optimization of wire electrical discharge machining based on response surface methodology. J Braz Soc Mech Sci Eng. 2014;36:301–13. https://doi.org/10.1007/s40430-013-0079-x.
11. Abdallah R, Soo SL, Hood R. A feasibility study on wire electrical discharge machining of carbon fibre reinforced plastic composites. Procedia Cirp. 2018;77:195–8. https://doi.org/10.1016/j.procir.2018.08.284.
12. Abdallah R, Soo SL, Hood R. The influence of cut direction and process parameters in wire electrical discharge machining of carbon fibre–reinforced plastic composites. Int J Adv Manuf Technol. 2021;113(5):1699–716. https://doi.org/10.1007/s00170-021-06641-2.
13. Abdallah R, Hood R, Soo SL. The machinability characteristics of multidirectional CFRP composites using high-performance wire EDM electrodes. J Compos Sci. 2022;6(6):159. https://doi.org/10.3390/jcs6060159.
14. Wu C, et al. Preheating assisted wire EDM of semi-conductive CFRPs: principle and anisotropy. J Mater Process Technol. 2021;288: 116915. https://doi.org/10.1016/j.jmatprotec.2020.116915.
15. Anbalagan A, Venugopal A, Anthony XM, Pazhani A and Batako A, "Novel machining configuration of carbon fibre reinforced polymer (CFRP) using wire electric discharge machining (WEDM)," In *International Conference on Intelligent Systems in Production Engineering and Maintenance*, 2023: Springer, pp. 16–24, doi: https://doi.org/10.1007/978-3-031-44282-7_2.
16. Ablyaz TR, Shlykov ES, Muratov KR, Sidhu SS. Analysis of wire-cut electro discharge machining of polymer composite materials. Micromachines. 2021;12(5):571. https://doi.org/10.3390/mi12050571.
17. Kamenskikh AA, et al. Recent trends and developments in the electrical discharge machining industry: a review. J Manuf Mater Process. 2023;7(6):204. https://doi.org/10.3390/jmmp7060204.
18. Dutta H, Debnath K, Sarma DK. A study of wire electrical discharge machining of carbon fibre reinforced plastic. In: Advances in unconventional machining and composites. Cham: Springer; 2020. p. 451–60.

19. Dutta, K. Debnath, and D. K. Sarma, "Investigation on cutting of thin carbon fiber-reinforced polymer composite plate using sandwich electrode-assisted wire electrical-discharge machining," *Proceedings of the institution of mechanical engineers, part E: journal of process mechanical engineering,* vol. 235, no. 5, pp. 1628-1638, 2021, doi: https://doi.org/10.1177/09544089211013318.

20. Wang S-M, Wu J-X, Gunawan H, Tu R-Q. Optimization of machining parameters for corner accuracy improvement for WEDM processing. Appl Sci. 2022;12(20):10324. https://doi.org/10.3390/app122010324.

21. Puri A, Bhattacharyya B. An analysis and optimisation of the geometrical inaccuracy due to wire lag phenomenon in WEDM. Int J Mach Tools Manuf. 2003;43(2):151–9. https://doi.org/10.1016/S0890-6955(02)00158-X.

22. Chen Z, Huang Y, Zhang Z, Li H, Ming WY, Zhang G. An analysis and optimization of the geometrical inaccuracy in WEDM rough corner cutting. Int J Adv Manuf Technol. 2014;74:917–29. https://doi.org/10.1007/s00170-014-6002-5.

23. Yang LJ, Dang XN. Analysis of the corner error in WEDM. Appl Mech Mater. 2010;37:146–9. https://doi.org/10.4028/www.scientific.net/AMM.37-38.146.

24. Abyar H, Abdullah A, Akbarzadeh A. Analyzing wire deflection errors of WEDM process on small arced corners. J Manuf Process. 2018;36:216–23. https://doi.org/10.1016/j.jmapro.2018.10.002.

25. Dodun O, Gonçalves-Coelho AM, Slătineanu L, Nagîţ G. Using wire electrical discharge machining for improved corner cutting accuracy of thin parts. Int J Adv Manuf Technol. 2009;41(9–10):858. https://doi.org/10.1007/s00170-008-1531-4.

26. Ali L, Imran SH, Khan WA and Ali H, "Optimization of Process Parameters for Precise Corner Accuracy in Wire Electric Discharge Machining of AISI D2 Tool Steel," 2023, doi: https://doi.org/10.21203/rs.3.rs-2718065/v1.

27. Saha S, Maity SR, Dey S. Machinability study of A286 superalloy for complex profile generation through wire electric discharge machining. Arab J Sci Eng. 2023;48(3):3241–53. https://doi.org/10.1007/s13369-022-07028-5.

28. Ishfaq K, Zahoor S, Khan SA, Rehman M, Alfaify A, Anwar S. Minimizing the corner errors (top and bottom) at optimized cutting rate and surface finish during WEDM of Al6061. Eng Sci Technol, Int J. 2021;24(4):1027–41. https://doi.org/10.1016/j.jestch.2021.01.008.

29. Yan H, Bakadiasa KD, Chen Z, Yan Z, Zhou H, Han F. Attainment of high corner accuracy for thin-walled sharp-corner part by WEDM based on magnetic field-assisted method and parameter optimization. Int J Adv Manuf Technol. 2020;106:4845–57. https://doi.org/10.1007/s00170-020-04966-y.

30. Zhang Y, et al. Simulation and experimental investigations of complex thermal deformation behavior of wire electrical discharge machining of the thin-walled component of Inconel 718. J Mater Process Technol. 2019;270:306–22. https://doi.org/10.1016/j.jmatprotec.2019.02.020.

31. Zhang Y, Zhang G, Zhang Z, Zhang Y, Huang Y. Effect of assisted transverse magnetic field on distortion behavior of thin-walled components in WEDM process. Chin J Aeronaut. 2022;35(2):291–307. https://doi.org/10.1016/j.cja.2020.10.034.

32. Rajkumar K, Balasubramaniyan C, Dhananchezian M, Ramraji K. Analysis of triangular WEDM cut corner inaccuracy of aluminium composite mold material. Mater Today: Proc. 2020;22:1341–50. https://doi.org/10.1016/j.matpr.2020.01.427.

33. Mandal K, Bose D, Mitra S, Sarkar S. Experimental investigation of process parameters in WEDM of Al 7075 alloy. Manuf Rev. 2020;7:30. https://doi.org/10.1051/mfreview/2020021.

34. Mandal K, Sekh M, Bose D, Mitra S, Sarkar S. Influence of dielectric conductivity on corner error in wire electrical discharge machining of Al 7075 alloy. Proc Inst Mech Eng C J Mech Eng Sci. 2021;235(20):5043–56. https://doi.org/10.1177/0954406220978268.

35. Ebisu T, Kawata A, Okamoto Y, Okada A, Kurihara H. Influence of jet flushing on corner shape accuracy in wire EDM. Procedia CIRP. 2018;68:104–8. https://doi.org/10.1016/j.procir.2017.12.031.

36. Abyar H, Abdullah A, Shafaroud AA. Theoretical and experimental analysis of machining errors on small arced corners during WEDM finishing stages. Mach Sci Technol. 2019;23(5):734–57. https://doi.org/10.1080/10910344.2019.1575410.

37. Chen Z, Zhang G. Study on magnetic field distribution and electro-magnetic deformation in wire electrical discharge machining sharp corner workpiece. Int J Adv Manuf Technol. 2018;98:1913–23. https://doi.org/10.1007/s00170-018-2260-y.

38. Selvakumar G, Bravilin Jiju K, Sarkar S, Mitra S. Enhancing die corner accuracy through trim cut in WEDM. Int J Adv Manuf Technol. 2016;83:791–803. https://doi.org/10.1007/s00170-015-7606-0.

39. Selvakumar G, Thiruppathi Kuttalingam K, Selvaraj M, Manohar J. Enhancing die corner accuracy using path modification strategy in wire electrical discharge machining of Monel 400. Proc Inst Mech Eng, Part C. 2018;232(2):207–16. https://doi.org/10.1177/0954406216679436.

40. Selvakumar G, Balasubramanian V, Lenin N. Investigation on corner accuracy in wire cut EDM of AISI D3 tool steel. Int J Rapid Manuf. 2020;9(1):58–70. https://doi.org/10.1504/IJRAPIDM.2020.104426.

41. Chakraborty S, Mitra S, Bose D. Experimental investigation on enhancing die corner accuracy during powder mixed wire EDM of Ti6Al4V. Mater Today: Proc. 2021;38:3097–102. https://doi.org/10.1016/j.matpr.2020.09.491.

42. Chaudhari R, et al. Multi-response optimization of Al2O3 nanopowder-mixed wire electrical discharge machining process parameters of nitinol shape memory alloy. Materials. 2022;15(6):2018. https://doi.org/10.3390/ma15062018.

43. Pratap P, Kumar J, Verma RK. Experimental investigation and optimization of process parameters during electric discharge machining of Inconel X-750. Multiscale and Multidisciplinary Modeling, Exper Des. 2020;3(3):161–71. https://doi.org/10.1007/s41939-020-00069-z.

44. Kumar J, Verma RK. Multiple response optimization in machining (milling) of graphene oxide-doped epoxy/CFRP composite using CoCoSo-PCA: a novel hybridization approach. J Adv Manuf Syst. 2021;20(02):423–46. https://doi.org/10.1142/S0219686721500207.

45. Nair H, et al. Experimental investigation on material removal rate, kerf width, surface roughness and the dimensional accuracy the accuracy of hole in Inconel 718 using wire electric discharge. Proc Inst Mech Eng. 2022. https://doi.org/10.1177/09544089221096025.

46. Kumar H, Manna A, Kumar R. Modeling and desirability approach-based multi-response optimization of WEDM parameters in machining of aluminum metal matrix composite. J Brazilian Soc Mech Sci Eng. 2018;40(9):458. https://doi.org/10.1007/s40430-018-1368-1.

47. Jogendra K, Verma RK, Mondal AK. Predictive modeling and machining performance optimization during drilling of polymer nanocomposites reinforced by graphene oxide/carbon fiber. Arch Mech Eng. 2020;67(2):229–58. https://doi.org/10.24425/ame.2020.131692.

48. "Shenzhen Sunlike Electronics Co., Ltd., which established at 2011. We are specialized in designing, developing, producing all kinds of carbon fiber products." https://www.made-in-china.com/showroom/chenxiaojunsunlike (accessed 2023.

49. Dereje T, Palani S, Desta M, Čep R. Experimental investigation into the influence of the process parameters of wire electric discharge machining using nimonic-263 superalloy. Materials. 2023;16(15):5440. https://doi.org/10.3390/ma16155440.

50. Zaman UKU, et al. Optimization of wire electric discharge machining (WEDM) process parameters for AISI 1045 medium carbon steel using taguchi design of experiments. Materials. 2022;15(21):7846. https://doi.org/10.3390/ma15217846.

51. Sekh M. Improvement of profile accuracy in WEDM—a novel technique. Accur Enhanc Technol Micromach Processes. 2020. https://doi.org/10.1007/978-981-15-2117-1_4.

52. Biswas S, Singh Y, Mukherjee M. An overview of wire electrical discharge machining (WEDM). Recent Adv Mech Eng. 2021;2020:643–52. https://doi.org/10.1007/978-981-15-7711-6_64.

53. Abyar H, Abdullah A, Akbarzadeh A. Prediction algorithm for WEDM arced path errors based on spark variable gap and nonuniform spark distribution models. J Manuf Sci Eng. 2019;141(1): 011011. https://doi.org/10.1115/1.4041779.

54. Singh J, Singh R, Kumar R. Review on effects of process parameters in wire cut EDM and wire electrode development. Int J Innov Res Sci Technol. 2016;2:701–6.

55. Pramanik D, Kuar A and Bose D, "Effects of wire EDM machining variables on material removal rate and surface roughness of Al 6061 alloy," in *Renewable Energy and its Innovative Technologies: Proceedings of ICEMIT 2017, Volume 1*, 2019: Springer, pp. 231–241, doi: https://doi.org/10.1007/978-981-13-2116-0_19.

56. Sagbas A. "Analysis and optimization of process parameters in wire electrical discharge machining based on RSM: A Case Study," in *Response Surface Methodology-Research Advances and Applications*: IntechOpen, 2022.doi: https://doi.org/10.5772/intechopen.107539.

57. Plaza S, Ortega N, Sanchez JA, Pombo I, Mendikute A. Original models for the prediction of angular error in wire-EDM taper-cutting. Int J Adv Manuf Technol. 2009;44(5):529–38. https://doi.org/10.1007/s00170-008-1842-5.

58. Ahmad B, Fitzpatrick ME. Minimization and mitigation of wire EDM cutting errors in the application of the contour method of residual stress measurement. Metall Mater Trans A. 2016;47(1):301–13. https://doi.org/10.1007/s11661-015-3231-7.

59. Yu J, et al. A confidence interval-based process optimization method using second-order polynomial regression analysis. Processes. 2020;8(10):1206. https://doi.org/10.3390/pr8101206.

60. Derringer G, Suich R. Simultaneous optimization of several response variables. J Qual Technol. 1980;12(4):214–9. https://doi.org/10.1080/00224065.1980.11980968.

Publisher's Note Springer Nature remains neutral with regard to jurisdictional claims in published maps and institutional affiliations.